Ultrafast all-optical switching in a silicon-based plasmonic nanoring resonator

S. Sederberg,* D. Driedger, M. Nielsen, and A.Y. Elezzabi

Department of Electrical and Computer Engineering, University of Alberta, Edmonton, Alberta, T6G 2V4, Canada
**shawns@ualberta.ca*

Abstract: A silicon-based plasmonic nanoring resonator is proposed for ultrafast, all-optical switching applications. Full-wave numerical simulations demonstrate that the photogeneration of free carriers enables ultrafast switching of the device by shifting the transmission minimum of the resonator with a switching time of 3 ps. The compact 1.00 μm^2 device footprint demonstrates the potential for high integration density plasmonic circuitry based on this device geometry.

OCIS codes: (240.6680) Surface plasmons; (230.7370) Waveguides; (320.0320) Ultrafast optics; (250.5403) Optoelectronics, plasmonics; (230.5750) Optical devices, resonators.

References and links

1. S. I. Bozhevolnyi, V. S. Volkov, E. Devaux, J.-Y. Laluet, and T. W. Ebbesen, "Channel plasmon subwavelength waveguide components including interferometers and ring resonators," Nature **440**(7083), 508–511 (2006).
2. E. Ozbay, "Plasmonics: merging photonics and electronics at nanoscale dimensions," Science **311**(5758), 189–193 (2006).
3. T. Nikolajsen, K. Leosson, and S. I. Bozhevolnyi, "Surface plasmon polariton based modulators and switches operating at telecom wavelengths," Appl. Phys. Lett. **85**(24), 5833–5836 (2004).
4. J. Gosciniak, S. I. Bozhevolnyi, T. B. Andersen, V. S. Volkov, J. Kjelstrup-Hansen, L. Markey, and A. Dereux, "Thermo-optic control of dielectric-loaded plasmonic waveguide components," Opt. Express **18**(2), 1207–1216 (2010).
5. D. J. Bergman and M. I. Stockman, "Surface plasmon amplification by stimulated emission of radiation: quantum generation of coherent surface plasmons in nanosystems," Phys. Rev. Lett. **90**(2), 027402 (2003).
6. M. Ambati, S. H. Nam, E. Ulin-Avila, D. A. Genov, G. Bartal, and X. Zhang, "Observation of stimulated emission of surface plasmon polaritons," Nano Lett. **8**(11), 3998–4001 (2008).
7. M. T. Hill, M. Marell, E. S. P. Leong, B. Smalbrugge, Y. Zhu, M. Sun, P. J. van Veldhoven, E. J. Geluk, F. Karouta, Y.-S. Oei, R. Nötzel, C.-Z. Ning, and M. K. Smit, "Lasing in metal-insulator-metal sub-wavelength plasmonic waveguides," Opt. Express **17**(13), 11107–11112 (2009).
8. I. De Leon and P. Berini, "Amplification of long-range surface plasmons by a dipolar gain medium," Nat. Photonics **4**(6), 382–387 (2010).
9. J. A. Dionne, K. Diest, L. A. Sweatlock, and H. A. Atwater, "PlasMOStor: a metal-oxide-Si field effect plasmonic modulator," Nano Lett. **9**(2), 897–902 (2009).
10. K. F. MacDonald, Z. L. Sámson, M. I. Stockman, and N. I. Zheludev, "Ultrafast active plasmonics," Nat. Photonics **3**(1), 55–58 (2009).
11. K. J. Chau, S. E. Irvine, and A. Y. Elezzabi, "A gigahertz surface magneto-plasmon optical modulator," IEEE J. Quantum Electron. **40**(5), 571–579 (2004).
12. A. Y. Elezzabi, Z. Han, S. Sederberg, and V. Van, "Ultrafast all-optical modulation in silicon-based nanoplasmonic devices," Opt. Express **17**(13), 11045–11056 (2009).
13. J. N. Caspers, N. Rotenberg, and H. M. van Driel, "Ultrafast silicon-based active plasmonics at telecom wavelengths," Opt. Express **18**(19), 19761–19769 (2010).
14. M. V. Ermolenko, O. V. Buganov, S. A. Tikhomirov, V. V. Stankevich, S. V. Gaponenko, and A. S. Shulenkov, "Ultrafast all-optical modulator for 1.5 μm controlled by Ti:Al_2O_3 laser," Appl. Phys. Lett. **97**(7), 073113 (2010).
15. S. Sederberg, V. Van, and A. Y. Elezzabi, "Monolithic integration of plasmonic waveguides into a complimentary metal-oxide-semiconductor- and photonic-compatible platform," Appl. Phys. Lett. **96**(12), 121101 (2010).
16. B. E. Little, S. T. Chu, H. A. Haus, J. Foresi, and J.-P. Laine, "Microring resonator channel dropping filters," J. Lightwave Technol. **15**(6), 998–1005 (1997).
17. A. V. Krasavin and A. V. Zayats, "Electro-optic switching element for dielectric-loaded surface plasmon polariton waveguides," Appl. Phys. Lett. **97**(4), 041107 (2010).
18. F. E. Doany, D. Grischkowsky, and C. C. Chi, "Carrier lifetime versus ion-implantation dose in silicon on sapphire," Appl. Phys. Lett. **50**(8), 460–462 (1987).

#154430 - $15.00 USD Received 9 Sep 2011; revised 14 Oct 2011; accepted 25 Oct 2011; published 3 Nov 2011

19. Y. Feng, M. Feser, A. Lyon, S. Rishton, X. Zeng, S. Chen, S. Sassolini, and W. Yun, "Nanofabrication of high aspect ratio 24 nm x-ray zone plates for x-ray imaging applications," J. Vac. Sci. Technol. B **25**(6), 2004 (2007).
20. M. A. Mohammad, T. Fito, J. Chen, M. Aktary, M. Stepanova, and S. K. Dew, "Interdependence of optimum exposure dose regimes and the kinetics of resist dissolution for electron beam nanolithography of polymethylmethacrylate," J. Vac. Sci. Technol. B **28**(1), L1 (2010).
21. M. A. Mohammad, S. K. Dew, S. Evoy, and M. Stepanova, "Fabrication of sub-10 nm silicon carbon nitride resonators using a hydrogen silsesquioxane mask prepared by electron beam lithography," Microelectron. Eng. **88**(8), 2338–2341 (2011).
22. S. Zhu, T. Y. Liow, G. Q. Lo, and D. L. Kwong, "Silicon-based horizontal nanoplasmonic slot waveguides for on-chip integration," Opt. Express **19**(9), 8888–8902 (2011).
23. S. Zhu, T. Y. Liow, G. Q. Lo, and D. L. Kwong, "Fully complimentary metal-oxide-semiconductor compatible nanoplasmonic slot waveguides for silicon electronic photonic integrated circuits," Appl. Phys. Lett. **98**(2), 021107 (2011).
24. Y. Song, J. Wang, Q. Li, M. Yan, and M. Qiu, "Broadband coupler between silicon waveguide and hybrid plasmonic waveguide," Opt. Express **18**(12), 13173–13179 (2010).
25. Z. Han, A. Y. Elezzabi, and V. Van, "Experimental realization of subwavelength plasmonic slot waveguides on a silicon platform," Opt. Lett. **35**(4), 502–504 (2010).
26. P. A. Schumann, Jr. and R. P. Phillips, "Comparison of classical approximations to free carrier absorption in semiconductors," Solid-State Electron. **10**(9), 943–948 (1967).

1. Introduction

The last several decades have witnessed the growth and maturing of complex, high-bandwidth fiber optics networks. While these optical networks have greatly enhanced data transmission capabilities, the optical signals must be converted to electrical signals when an electronic device receives the data. Typical electronic devices rely on charge transport, resulting in a bandwidth that is inferior to that of the delivering optical networks'. This limitation has motivated countless research efforts into the development of all-optical integrated circuitry that would perform the same functions as their electronic counterparts, but with enhanced speed and efficiency. Although the field of photonics has experienced substantial developments in recent years, the minimum dimensions of photonic devices are limited by the diffraction limit of the optical radiation, and are typically large compared to electronic devices.

More recently, it has been demonstrated that nanoscale waveguides including metallic features can support plasmonic modes and may be designed to have sub-diffraction dimensions [1]. Based on demonstrations of high integration density and sharp bending radii, it has been proposed that plasmonic waveguides could form a basis for the next generation chip-scale technology [2]. Moreover, the high modal confinement offered by plasmonic waveguides enhances incident electric fields and allows for efficient access to nonlinear optical effects. Previous approaches to plasmonic signal modulation have involved thermo-optic effects [3,4], plasmonic amplifiers [5–8], charge redistribution in n^+-Si via electric field application [9], radiation-induced interband transitions in aluminum [10], magnetic field modulation of surface magneto-plasmon waves [11], and photogenerated free-carrier modulation in semiconductors [12–14].

Recently, it has been proposed that silicon-based plasmonic circuitry would allow for compatibility with existing complimentary metal-oxide-semiconductor (CMOS) process techniques, allowing for monolithic integration of electronic and plasmonic devices [15]. In a previous investigation, it was demonstrated that a five-layer slab waveguide incorporating ion-implanted silicon (II-Si) could be used to achieve switching times of 5 ps and an *on-off* contrast ratio of 35 dB [12]. By end-firing above-bandgap radiation into the waveguide, free carriers were excited, introducing loss in the silicon layers and modulating the transmission of a signal with a wavelength, λ = 1550 nm. In a subsequent experiment, a plasmonic grating structure incorporating silicon features was used to demonstrate this principle [13]. By exciting the grating with above-bandgap radiation, the coupling resonance for a telecommunications wavelength signal was shifted by more than its width, switching the coupling to the *"off"* state. Non-treated silicon was used in the grating, and a recovery time of 103 ps was observed.

#154430 - $15.00 USD Received 9 Sep 2011; revised 14 Oct 2011; accepted 25 Oct 2011; published 3 Nov 2011

Although these structures effectively demonstrate the principle of plasmonic signal modulation by exciting free carriers and inducing loss in the adjacent silicon layers, these devices are quite bulky. In the case of the slab waveguide, the device occupied a footprint of 8.25 μm^2, while the grating structure occupied a footprint of 0.5 mm^2. In order to reduce the dimensions of these devices to a scale that may be suitable for high integration density, it is necessary to investigate alternative device configurations that allow for similar switching and modulation properties, but having a reduced footprint. One structure that has been investigated for applications in silicon photonics is the microring resonator [16]. Recently, it was numerically demonstrated that the electro-optic effect could be used to switch a polymer-loaded nanoscale ring resonator from the *"on"* state to the *"off"* state [17]. Although experiments have verified the basic passive functionality of a plasmonic microring resonator [2], a compact all-optical plasmonic nanoscale ring resonator switching device has not yet been demonstrated experimentally.

In this investigation, we numerically demonstrate ultrafast all-optical switching in a silicon-based plasmonic nanoring resonator. By coupling above-bandgap ultrafast optical pulses into the nanoring resonator, photogenerated free carriers modify the complex refractive index of the nanoring resonator. In doing so, the optical path length of the resonator is altered, transmission minima of the nanoring resonator are shifted, and the power transmission of the signal wavelength is modulated.

2. Device Geometry

The nanoring resonator and associated circuitry are based on dielectric-loaded plasmonic waveguides. Signals in the S-band are transmitted through silicon-loaded plasmonic waveguides, whereas above-bandgap ultrafast optical pulses are routed by SiO_2-loaded plasmonic waveguides. Although the indirect bandgap of silicon limits the electron-hole (e-h) recombination time to timescales from nanoseconds to hundreds of picoseconds (depending on the growth or deposition technique and length scale of the device), it is possible to reduce the e-h recombination time further by implanting O^+ ions into the Si, introducing carrier trap centers and reducing the carrier lifetime to 600 fs [18]. In this investigation, we assume that the nanoring resonator is composed of O^+ ion implanted Si (II-Si) and has a free carrier recombination time of τ_c = 1ps in order to enhance the switching speed of the device.

A schematic of the device is shown in Fig. 1. The plasmonic waveguides are formed on a silver film having a thickness t_{Ag} = 100 nm. The width of the waveguides is uniform, w_{Si} = w_{SiO2} = 100 nm. Based on iterative design discussed in a subsequent section, the nanoring is given a radius, r = 560 nm, which corresponds to a footprint area of 1.00 μm^2. An input bus plasmonic waveguide carrying S-band signals couples radiation to the resonator and is separated from the resonator by a gap g_{Si} = 25 nm. Above-bandgap femtosecond optical pulses centered at λ = 800 nm are coupled into the resonator by a waveguide that is concentric to the resonator and offset from it by a gap, g_{SiO2} = 20 nm.

These devices can be fabricated by depositing a silver film onto a SiO_2 substrate. The silicon waveguides can be created by lithographically defining a mask, dry etching through the silver film, depositing α-silicon, and removing the deposited film in the masked areas. A second layer of lithography may be performed to define the SiO_2-loaded plasmonic waveguides in the same manner. Notably, any misalignment in this layer will alter the

#154430 - $15.00 USD Received 9 Sep 2011; revised 14 Oct 2011; accepted 25 Oct 2011; published 3 Nov 2011

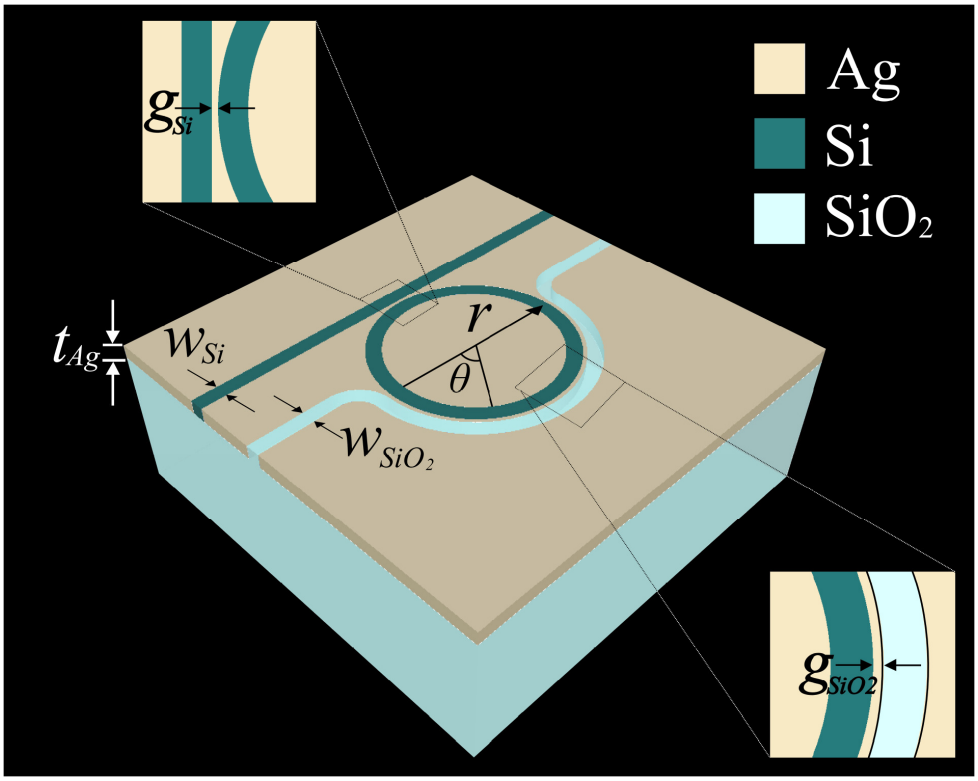

Fig. 1. Schematic depiction of the device geometry. The nanoring is designed to have a radius, r = 560 nm, silver film thickness, t_{Ag} = 100 nm, input coupler separation, g_{Si} = 25 nm, modulation coupler separation, g_{SiO2} = 20 nm, and uniform waveguide widths, $w_{Si} = w_{SiO2}$ = 100 nm.

coupling efficiency of the above-bandgap pump pulses. Nanofabrication techniques for such small feature sizes are possible using electron beam lithography and systematic process development [19–21]. Focused ion beam may be used to correct certain process defects.

3. Passive Operation

Due to the sub-diffraction dimensions of this nanoscale plasmonic device and the complex nature of its geometry, full-wave numerical simulations are used as the primary design tool. Three-dimensional finite-difference time-domain simulations with broadband dielectric functions fit to experimental data were used to model the behavior of the resonator. In order to understand the passive operation of the nanoring structure, the silicon bus plasmonic waveguide was excited by a broadband pulse centered at λ = 1550 nm, a full-width at half-maximum, *FWHM* = 390 nm, and the plasmonic mode profile shown in Fig. 2(a). This mode has an effective refractive index of $n_{eff,Si}$ = 3.382 at λ = 1515 nm and undergoes a propagation loss of 4.371 dB/μm. Although the loss of this mode is quite high, it has been shown that plasmonic devices may be coupled together with low-loss photonic waveguides with coupling efficiencies up to 80% [15,22–25]. This scheme may be used to propagate signals over long distances where plasmonic waveguides may be too lossy. The transmission spectrum of the nanoring resonator is calculated by recording the electric fields in the silicon bus plasmonic waveguide at a distance of 1.0 μm before the nanoring resonator and 0.9 μm beyond the nanoring resonator. By Fourier transforming the time domain signals, and normalizing the spectrum transmitted beyond the nanoring resonator to the spectrum that excites the nanoring resonator, the broadband transmission spectrum is obtained and is shown in Fig. 2(b). By

#154430 - $15.00 USD Received 9 Sep 2011; revised 14 Oct 2011; accepted 25 Oct 2011; published 3 Nov 2011

iterative design of the nanoring resonator radius, r, and coupling gaps, g_{Si} and g_{SiO2}, a transmission minimum is obtained at a wavelength of λ = 1515 nm for a ring radius of r = 560 nm.

The performance of the SiO_2 coupling plasmonic waveguide is investigated by exciting the SiO_2 plasmonic waveguide with a broadband pulse centered at λ = 800 nm, a full-width at half-maximum, FWHM = 94 nm, and the plasmonic mode profile shown in Fig. 2(c). This mode has an effective index of $n_{eff,SiO2}$ = 1.742 at a pump wavelength of λ = 800 nm and undergoes a propagation loss of 2.292 dB/μm. The electric fields are recorded at ten ring angles in the range $0° \le \theta \le 135°$ and the power, P, coupled to the ring at each angle is normalized to the input power, as shown in Fig. 2(d). These data points are fit with a skewed Gaussian function of the form,

$$P = \frac{a}{\sqrt{2\pi}} \exp\left[-\frac{b}{2}(\theta - c)^2\right] \times \left[1 + erf\left[\frac{d}{\sqrt{2}}(\theta - e)\right]\right] \quad (1)$$

where {a,b,c,d,e} = {0.495, 1.63×10^{-3}, 28, 0.12, 5.0} and an R-squared fit, R^2 = 0.93. It is important to note that the power is significantly reduced beyond θ = 135°, and minimal power remains to propagate around the nanoring beyond the SiO_2 bus waveguide. For

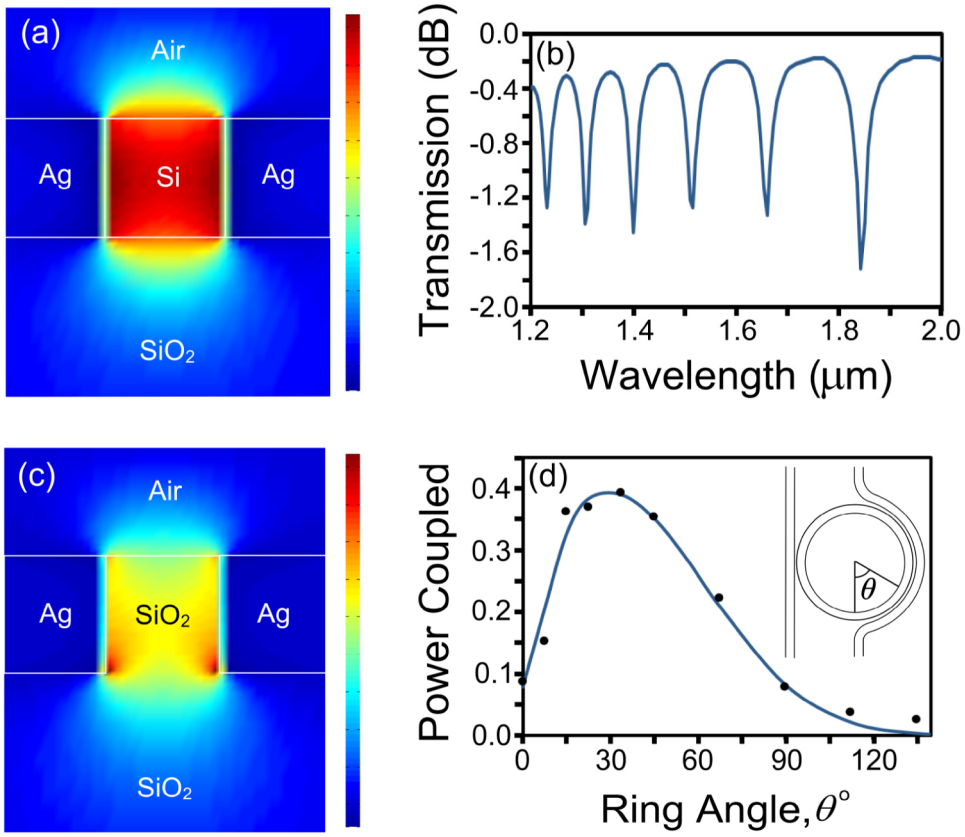

Fig. 2. Electric field intensity distribution of the excited mode in a silicon-loaded plasmonic waveguide at λ = 1515 nm. (b) Broadband transmission through silicon bus plasmonic waveguide coupled to nanoring resonator. (c) Electric field intensity distribution of the excited mode in a SiO_2-loaded plasmonic waveguide at λ = 800 nm. (d) Pump power (λ = 800 nm) coupled to nanoring versus nanoring angle, θ (see inset). The coupled power is normalized to the input power. A skewed Gaussian function is fitted to the recorded points.

#154430 - $15.00 USD Received 9 Sep 2011; revised 14 Oct 2011; accepted 25 Oct 2011; published 3 Nov 2011

$0° \le \theta \le 35°$ the power coupled to the nanoring increases with θ due to the increasing coupling length between the SiO_2 waveguide and the Si nanoring. However, the above-bandgap radiation undergoes substantial loss as it continues to propagate around the silicon nanoring and gradually decays by $\theta = 135°$. Although the plasmonic waveguide introduces unwanted dispersion to the pump pulse, the interaction length from $\theta = 0°$ to $\theta = 135°$ is $l = r\theta$ = 0.56μm*π*135°/180° = 1.3 μm and only broadens the pulse slightly from τ_p = 10 fs to τ_p = 12 fs by the time it reaches $\theta = 135°$. Notably, this is still much shorter than the electron-hole recombination time, which is the process that limits the switching time of the device. Furthermore, a majority of the free carriers are excited at $\theta \le 60°$, where less dispersion will have accumulated.

4. Ultrafast Active Operation

As discussed above, the nanoring is designed with a transmission minimum at λ = 1515 nm. By coupling an ultrafast above-bandgap radiation pulse into the nanoring, free carriers are excited and the complex refractive index in the nanoring is altered, and thus, the transmission minimum is shifted to a new wavelength. The time-dynamics of the permittivity, $\varepsilon(t)$, of the silicon in the nanoring resonator are modeled by a frequency-dependent Drude-Lorentz model for a semiconductor,

$$\varepsilon(t) = \varepsilon'_b\left[1 - \frac{n(t)e^2 < \tau >^2}{\varepsilon'_b \varepsilon_0 m^* (1 + \omega^2 \tau >^2)}\right] - i\varepsilon'_b\left[\frac{\varepsilon''_b}{\varepsilon'_b} + \frac{n(t)e^2 < \tau >^2}{\varepsilon'_b \varepsilon_0 m^* \omega (1 + \omega^2 < \tau >^2)}\right] \quad (2)$$

where ε'_b = 12.1 and $\varepsilon''_b = 9.2 \times 10^{-4}$ are the real and imaginary component of the permittivity in the absence of free carriers (i.e. bound charges only), respectively, ε_0 is the permittivity of free space, ω is the frequency of radiation interacting with the semiconductor, e is the electronic charge, $m^* = 1.40 \times 10^{-31}$ kg is the effective mass of free carriers, $<\tau>$ = 10.6 fs is the average carrier-carrier relaxation time, and $n(t)$ is the density of free carriers in the conduction band generated by the above-bandgap pulse [26]. Notably, the permittivity, and therefore the complex refractive index, depends on the density of free carriers. For carrier densities above a critical value,

$$n_c = \frac{\varepsilon_0 \varepsilon'_b m^* (1 + \omega^2 < \tau >^2)}{e^2 < \tau >^2} \quad (3)$$

the real component of the permittivity becomes negative and the silicon behaves as a metal for radiation of frequency, ω. For silicon at λ = 1515 nm, $n_c = 9.106 \times 10^{20}$ cm^{-3}.

The free carriers are generated by a λ = 800 nm control pulse having a duration, τ_p = 10 fs, which is assumed to have a $sech^2$ temporal envelope. The dominant free carrier decay process is assumed to be recombination of e-h pairs at recombination centers in the II-Si layers at a characteristic time, τ_c. Therefore, the instantaneous free carrier density can be obtained from the equation:

$$\frac{\partial n(t)}{\partial t} = \frac{n_0}{\tau_p} \sec h^2\left(\frac{t - t_0}{\tau_p}\right) - \frac{n(t)}{\tau_c} \quad (4)$$

where n_0 is the maximum carrier concentration at the peak of the control pulse when $t = t_0$, τ_p = 10 fs is the duration of the control pulse, and τ_c = 1 ps is the characteristic carrier lifetime in the II-Si waveguide. From hereon in, all pump powers are referred to in terms of the maximum carrier concentration relative to the critical carrier density, i.e. n_0/n_c. As a conservative estimate, we may assume that angles in the range, $0° \le \theta \le 180°$, are pumped uniformly, which corresponds to a pumping volume, $V = 1.76 \times 10^{-14}$ cm^3. Furthermore, a pumping photon with λ_p = 800 nm has an energy $E_p = hc/\lambda_p = 2.48 \times 10^{-19}$ J/photon.

#154430 - $15.00 USD Received 9 Sep 2011; revised 14 Oct 2011; accepted 25 Oct 2011; published 3 Nov 2011

Therefore, the total energy required to photogenerate a free carrier density of n_0 may be obtained from the equation,

$$E_{pump} = \eta E_p n_0 V \tag{5}$$

where η is the quantum efficiency of the photogeneration process, which we assume to be unity, i.e. $\eta = 1$.

Rather than applying a self-consistent solution of Maxwell's equations with Eqs. (2-4), which is an elegant, albeit time-consuming approach, we choose to separate the λ = 800 nm pump calculations from the λ = 1515 nm signal calculations. In this analysis, we assume that the λ = 1515 nm signal is a low-intensity signal and that we may ignore all $\chi(3)$ processes in silicon and that the λ = 1515 nm signal has no influence on itself or the λ = 800 nm pump. The presence of the λ = 800 nm pump does, however, alter the propagation of the λ = 1515 nm signal. Due to the short pump pulse duration (τ_p ~10 fs), it can be assumed that the permittivity function of silicon takes on an instantaneous change. Any influence of the pump pulse that is co-propagating with the probe signal (i.e. in angles $0° \le \theta \le 135°$) during the excitation occurs on a very short time scale relative to the picosecond switching time of the device and would not be significant. Due to the short pump pulse duration, the pump pulse couples to the ring and propagates along the ring in the same manner as it would in the absence of any nonlinear electric field effects. Since the interaction distance is short (l = 1.3μm), negligible pulse distortion will be incurred for these relatively low free carrier densities (n_0 ~$0.2n_c$).

The time required to build up the resonant response (or decay of the resonant response) in the ring resonator depends on its quality factor. In the present case, the transmission minimum at λ = 1515 nm has a quality factor of $Q = \omega/\Delta\omega_{FWHM}$ = 42.5, where ω is the central frequency of the resonance and $\Delta\omega_{FWHM}$ is the FWHM of the resonance. The photon lifetime of the resonator may then be calculated as $\tau_{lifetime} = Q/\omega$ = 34.2 fs. To assume a fixed permittivity (or plasma density), $\tau_{lifetime}$ must be very short such that during the buildup or decay of the radiation inside the ring resonator, there is minimal change in the refractive index and therefore, it can be taken as being constant. On a $\tau_{lifetime}$ = 34.2 fs timescale, the maximum percentage change in plasma density is calculated to be 3.4%, and accordingly, the maximum percentage change in the real and imaginary components of the refractive index are calculated to be 1.0% and 4.4%, respectively. Based on this relatively low change in the refractive index over the photon lifetime in the ring resonator, we may say that the refractive index is approximately constant over the photon lifetime in the ring resonator.

Based on this conclusion, we first calculate the refractive index at each point in the ring at each point in time. By simulating one temporal "snapshot" at a time for a fixed refractive index distribution in the ring, it is possible to calculate the power transmission of the ring as the resonant response of the ring resonator builds up over $\tau_{lifetime}$ = 34.2 fs. By performing these simulations at multiple "snapshots", it is possible to visualize the temporal response of the power transmitted by the ring as the free carriers are excited and gradually recombine.

In order to model the refractive index at each nanoring angle, θ, in the resonator at each instant in time, it is first necessary to determine the free carrier density as a function of nanoring angle. The free carrier density at each point in the nanoring is proportional to the intensity of above-bandgap radiation at that point. By selecting a maximum pump strength, n_0/n_c, coupled to the nanoring at $\theta = 35°$, the carrier density at each nanoring angle, θ, may be calculated from Eq. (1). The time-dynamics of the free carrier density at each angle may then be determined from Eq. (4), and finally, the time-dynamics of the permittivity (and therefore, refractive index) at each angle may be obtained from Eq. (2). Surface plots relating the real component of the refractive index to the nanoring angle, θ, and time, t, for pump strengths of

#154430 - $15.00 USD Received 9 Sep 2011; revised 14 Oct 2011; accepted 25 Oct 2011; published 3 Nov 2011

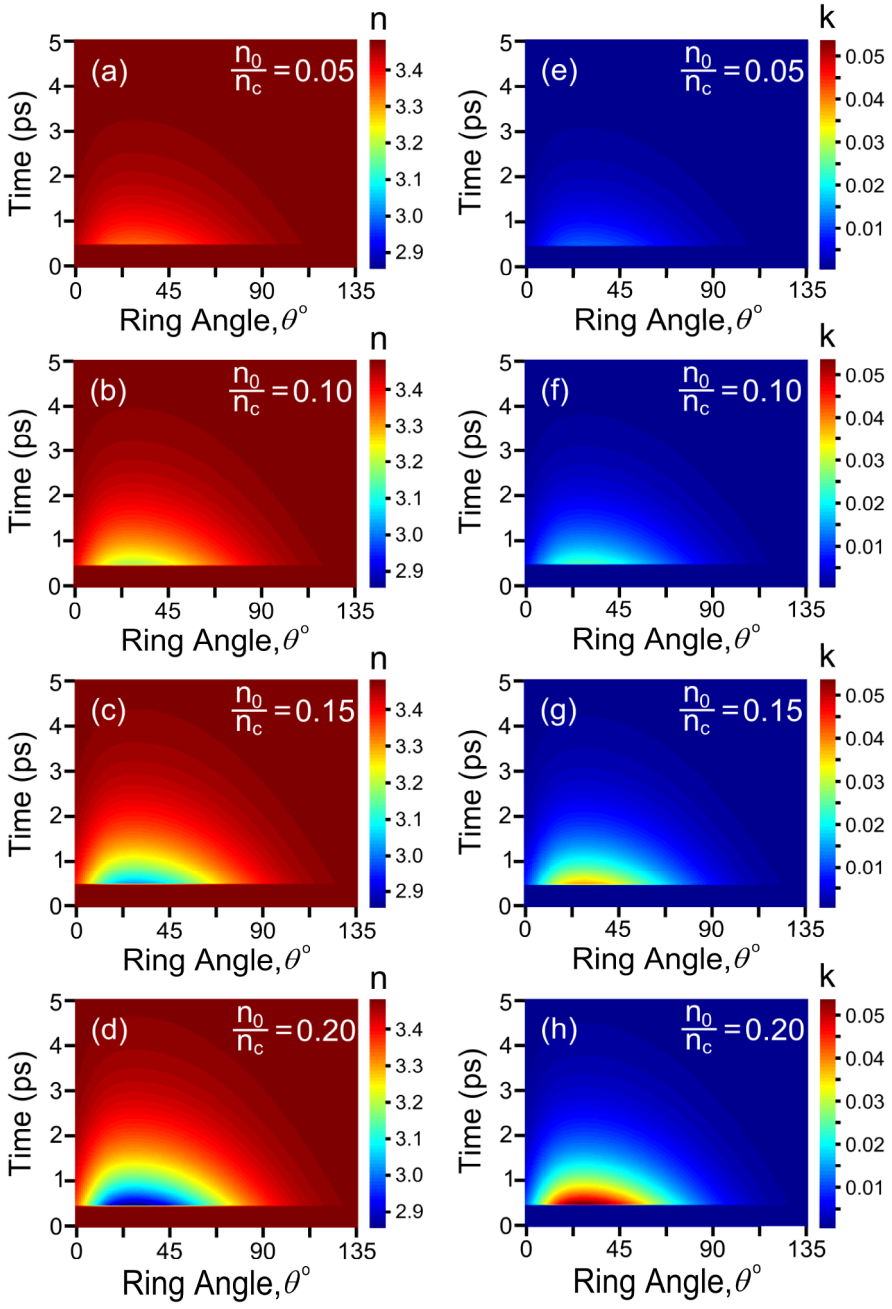

Fig. 3. Refractive index of silicon as a function of time and nanoring angle when excited by ultrafast above-bandgap pulses of τ_p = 10 fs duration at λ = 800 nm. The real component of the refractive index of II-Si in the ring is modeled for pump strengths of n_0/n_c = 0.05, 0.10, 0.15, and 0.20 in (a), (b), (c), and (d), respectively. The imaginary component of the refractive index of II-Si in the nanoring is modeled for pump strengths of n_0/n_c = 0.05, 0.10, 0.15, and 0.20 in (e), (f), (g), and (h), respectively.

n_0/n_c = 0.05, 0.10, 0.15, and 0.20 are shown in Figs. 3(a)-(d), respectively. Surface plots relating the imaginary component of the refractive index to the nanoring angle, θ, and time, t, for pump strengths of n_0/n_c = 0.05, 0.10, 0.15, and 0.20 are shown in Figs. 3(e)-(h), respectively. The time required to generate free carriers and alter the refractive index is very

#154430 - $15.00 USD Received 9 Sep 2011; revised 14 Oct 2011; accepted 25 Oct 2011; published 3 Nov 2011

short and is limited primarily by the duration of the excitation pulse. However, the time required for the material to recover to its non-excited state is longer and is limited by the e-h recombination time. After a recovery time of t = 3 ps, the material properties have returned to their non-excited state.

By applying these results to the II-Si of the nanoring resonator, it is possible to calculate the change in power transmission as the pumping strength is increased for signal radiation of a fixed wavelength, λ = 1515 nm. Substantial pump radiation is coupled to the nanoring for angles in the range, $0° \le \theta \le 168.75°$, and consequently, the refractive index of the nanoring will only undergo changes in these regions. The silicon of the nanoring resonator that falls in the range, $0° \le \theta \le 168.75°$, is divided into twelve segments, each of which is given its own optical properties based on data taken from Fig. 3. Finite-difference time-domain simulations are performed on ten different nanoring resonators, each with an angular-dependent refractive index representing a different free carrier distribution. Intensity distributions of the nanoring resonator and adjacent bus waveguides for pumping strengths of n_0/n_c = 0.00, 0.10, and 0.22 are shown in Figs. 4(a)-(c), respectively. Each of these intensity distributions is plotted on the same scale for ease of comparison. In the absence of pumping, the electric fields add destructively in the II-Si bus plasmonic waveguide and a minimal signal is transmitted. However, as the pump strength increases, fields begin to add constructively in the II-Si bus plasmonic waveguide and a strong transmitted signal is observed for the case of n_0/n_c = 0.22. Figure 4(d) shows the influence of the pumping strength on the position of the transmission

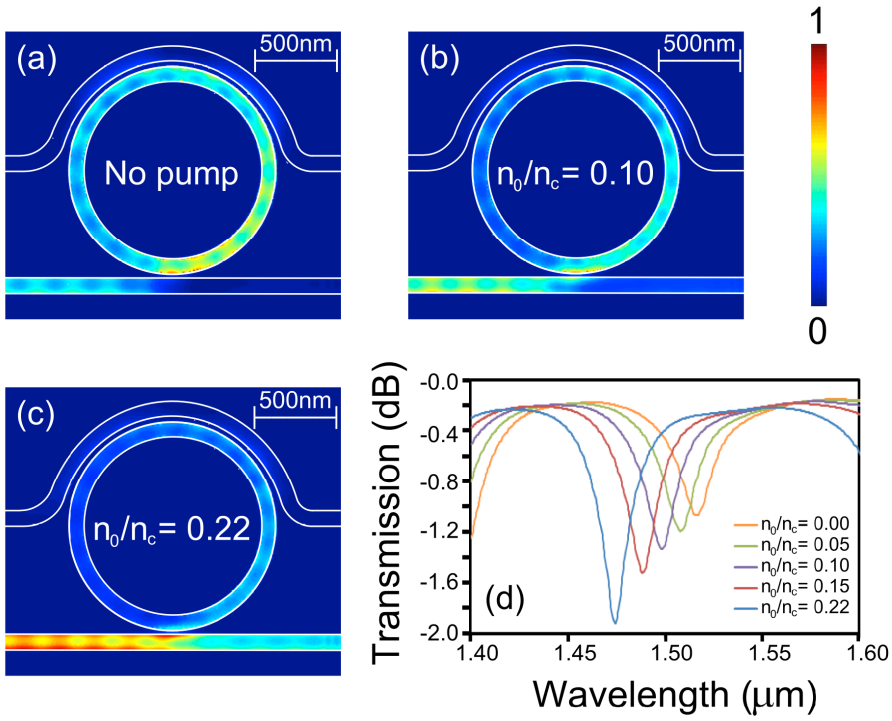

Fig. 4. (a) Intensity distribution of the nanoring resonator in the *"off"* state without any pump. (b) Intensity distribution of the ring resonator for a pump strength of n_0/n_c = 0.10. (c) Intensity distribution of the nanoring resonator in the *"on"* state, with a pump strength of n_0/n_c = 0.22. Each of the three intensity distributions is presented on the same scale. (d) Effect of the pump strength on the position of the transmission minimum.

#154430 - $15.00 USD Received 9 Sep 2011; revised 14 Oct 2011; accepted 25 Oct 2011; published 3 Nov 2011

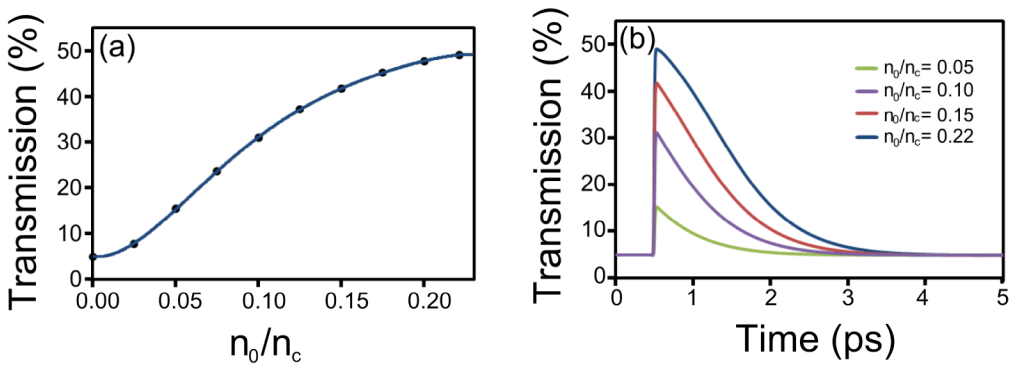

Fig. 5. (a) Dependence of the power transmission through II-Si bus waveguide on the pump strength. (b) Power transmission through the II-Si bus waveguide as a function of time for pump strengths of n_0/n_c = {0.05, 0.10, 0.15, 0.22}.

minimum. As the free carrier density increases, the optical path length of the nanoring resonator decreases and the transmission minimum shifts to the blue part of the spectrum. As a result, the adjacent transmission maximum shifts closer to the signal wavelength of λ = 1515 nm and the transmitted power increases.

The dependence of power transmitted on the maximum free carrier density in the nanoring is shown in Fig. 5(a), and is fit by a fifth-order polynomial with $R^2 = 1$. While a weak signal of 4.95% of the input signal strength is observed in the absence of pumping, the signal strength increases to 49% of the input signal strength for a pumping strength of $n_0/n_c = 0.22$. With knowledge of both the time-dynamics of free carriers (from Eq. (4) and the power transmitted through the II-Si bus plasmonic waveguide as a function of the maximum free carrier density in the nanoring, it is possible to visualize the time-dynamics of the power transmitted through the silicon bus waveguide simply by multiplying the data of Fig. 5(a) by the solution to Eq. (4). These dynamics are shown for pumping strengths of n_0/n_c = 0.05, 0.10, 0.15, and 0.22 in Fig. 5(b). Notably, the device is switched to the *"on"* state on a femtosecond timescale. After a time of 3 ps, the device has completely recovered to the *"off"* state. Based on these characteristic rise and fall times, a modulation frequency of 0.33 THz is possible using this structure. From Eq. (5), a pumping energy of E_{pump} = 0.88 pJ must be coupled to the nanoring resonator in order to switch the device to the *"on"* state (n_0/n_c = 0.22). When driven in a continuous manner, this translates to a power consumption of 290 mW. However, digital devices are typically used in short bursts as they participate in an isolated operation, and the actual power consumption is considerably lower. Therefore, the switching energy is a more meaningful figure to describe the energy efficiency of the device and is analogous to the power-delay product commonly reported for microelectronic devices.

5. Conclusions

A silicon-based plasmonic nanoring resonator has been designed and its behavior has been characterized via rigorous numerical simulations. Photogenerated free carriers are used to shift the transmission minimum of the resonator, shifting the device from the *"off"* state to the *"on"* state. The compact 1.00 μm^2 footprint of this device and its ultrafast switching time of 3 ps demonstrate its potential for high-density, ultrafast, all-optical plasmonic circuitry that, with the exception of the silver film, maintains compatibility with CMOS processing techniques.

Acknowledgements

This work was supported by the Natural Sciences and Engineering Research Council of Canada, Alberta Innovates, and the Canadian Research Chairs.

#154430 - $15.00 USD Received 9 Sep 2011; revised 14 Oct 2011; accepted 25 Oct 2011; published 3 Nov 2011